Three-Dimensional Quantitative Structure−Activity Relationship Study of the Cannabimimetic (Aminoalkyl)indoles Using Comparative Molecular Field Analysis

Joong-Youn Shim, Elizabeth R. Collantes,† and William J. Welsh*

Department of Chemistry and Center for Molecular Electronics, University of Missouri-St. Louis, St. Louis, Missouri 63121

Babu Subramaniam‡ and Allyn C. Howlett

Department of Pharmacological and Physiological Science, Saint Louis University School of Medicine, St. Louis, Missouri 63104

Michael A. Eissenstat§ and Susan J. Ward⊥

Sanofi Research Division, Sanofi-Winthrop, Collegeville, Pennsylvania 19426

Received May 15, 1998

The present study describes the implementation of comparative molecular field analysis (CoMFA) to develop two 3D-QSAR (quantitative structure-activity relationship) models (CoMFA models 1 and 2) of the cannabimimetic (aminoalkyl)indoles (AAIs) for CB_1 cannabinoid receptor binding affinity, based on pK_i values measured using radioligand binding assays that displace two different agonist ligands, [^{3}H]CP-55940 and [^{3}H]WIN-55212-2. Both models exhibited a strong correlation between the calculated steric−electrostatic fields and the observed biological activity for the respective training set compounds. In light of the basicity of the morpholine nitrogen in the AAIs, separate CoMFA models were built for the AAIs as unprotonated and protonated species. Comparison of the statistical parameters resulting from these CoMFA models failed to provide unequivocal evidence as to whether the AAIs are protonated or neutral as receptor-bound species. Although the training sets of CoMFA model 1 and CoMFA model 2 differed with respect to composition and to the choice of displacement radioligand in each biological assay, their CoMFA StDev*Coeff contour plots reveal similarities in terms of identifying those regions around the AAIs that are important for CB_1 cannabinoid receptor binding such as the sterically favored region around the C3 aroyl group and the sterically forbidden region around the indole ring. When the experimental pK_i values for the training set compounds to displace the AAI radioligand [^{3}H]WIN-55212-2 were plotted against the pK_i values as predicted for the same compounds to displace the cannabinoid radioligand [^{3}H]CP-55940, the correlation was moderately strong ($r = 0.73$). However, the degree of correlation may have been lowered by the structural differences in the compounds comprising the training sets for CoMFA model 1 and CoMFA model 2. Taken together, the results of this study suggest that the binding site region within the CB_1 cannabinoid receptor can accommodate a wide range of structurally diverse cannabimimetic analogues including the AAIs.

Introduction

The (aminoalkyl)indoles (AAIs), developed from the lead compound pravadoline (Figure 1), comprise a novel class of cannabinoid receptor agonists consisting of an indole nucleus substituted by an aminoalkyl group at position 1 and an aroyl group at position 3. Research conducted at Sterling Winthrop Research Institute demonstrated that pravadoline exhibits potent antinociceptive activity and inhibits brain cyclooxygenase as expected for a nonsteroidal antiinflammatory drug (NSAID).[1,2] In contrast to the classical NSAIDs, however, pravadoline displayed no gastrointestinal cytotoxicity and no antiinflammatory activity.[3] A series of pravadoline analogues have been developed that exhibit greater potency as antinociceptive agents but fail to block prostaglandin synthesis.[2,4] One structurally constrained analogue, [2,3-dihydro-5-methyl-3-[(4-morpholinyl)methyl]pyrrolo[1,2,3-*de*]-1,4-benzoxazin-6-yl](1-naphthyl)-methanone (WIN-55212-2), was found to bind to the CB_1 cannabinoid receptor in rat brain membranes with high affinity,[5] and [^{3}H]WIN-55212-2 (Chart 1) was used to develop a radioligand binding assay.[6] Other AAI analogues were also able to displace the potent cannabinoid ligand (1*R*,3*R*,4*R*)-3-[2-hydroxy-4-(1,1-dimethylheptyl)-phenyl]-4-(3-hydroxypropyl)cyclohexan-1-ol (CP-55940) binding to the CB_1 cannabinoid receptor with a level of potency that paralleled their ability to inhibit cerebellar adenylate cyclase activity, to reduce mouse vas deferens contractions, and to behave as analgesics in several

* Corresponding author.
† Present address: Monsanto, St. Louis, MO 63167.
‡ Present address: Palm Beach Neurogroup, Palm Beach Gardens, FL 33410.
§ Present address: Structural Biochemistry Program, SAIC, NCI-Frederick Cancer Research & Development Center, Frederick, MD 21702.
⊥ Present address: Wyeth-Ayerst Research, P.O. Box 8299, Philadelphia, PA 19101.

10.1021/jm980305c CCC: $15.00
Published on Web 10/15/1998

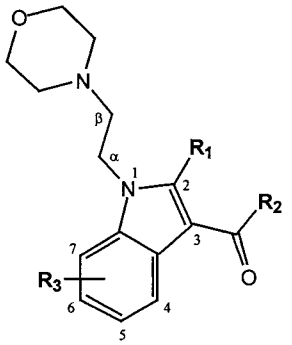

Compound Designation	R_1	R_2	R_3	pK_i (obsd.)	unprotonated		protonated	
					pK_i (calcd.)	Residual	pK_i (calcd.)	Residual
pravadoline	Me	*p*-OMe-phenyl	H	-3.40	--[l]	--	--[l]	--
2	H	*p*-OMe-phenyl	H	-2.49	--[l]	--	--[l]	--
4	H	7-benzofuryl	H	-1.15	--[l]	--	--[l]	--
8[a]	H	1-naphthyl	H	-1.61	--[l]	--	--[l]	--
9	H	1-naphthyl	H	-0.78	--[l]	--	--[l]	--
11	Me	1-naphthyl	H	-1.18	--[l]	--	--[l]	--
12[b]	H	1-naphthyl	H	-0.38	--[l]	--	--[l]	--
13[c]	H	1-naphthyl	H	0.02	--[l]	--	--[l]	--
15	Me	*o*-OMe-phenyl	H	-2.80	-2.99	0.19	-2.46	-0.34
16	Me	*p*-OMe-phenyl	6-Me	-3.17	-2.58	-0.59	-2.63	-0.54
17	Me	*p*-OMe-phenyl	7-Me	-3.08	-3.04	-0.04	-3.19	0.11
18	Me	*p*-OMe-phenyl	6-OMe	-3.06	-3.02	-0.04	-2.71	-0.35
19	Me	*p*-OMe-phenyl	7-F	-2.65	-2.89	0.24	-2.56	-0.09
20	Me	*p*-OMe-phenyl	6-Br	-2.61	-2.50	-0.11	-2.51	-0.10
21[d]	Me	*p*-OMe-phenyl	H	-2.69	-3.01	0.32	-2.97	0.28
22	Me	*m*-Me-phenyl	H	-2.68	-2.88	0.20	-2.82	0.14
23	Me	*p*-Me-phenyl	H	-3.15	-2.40	-0.75	-3.00	-0.15
24	Me	*m*-Cl-phenyl	H	-3.02	-2.72	-0.30	-3.04	0.02
25	Me	*p*-Et-phenyl	H	-2.38	-2.21	-0.17	-2.81	0.43
26	Me	*p*-*i*-Pr-phenyl	H	-2.95	-3.00	0.05	-3.17	0.21
27	Me	*o,m*-di-Me-phenyl	H	-2.47	-2.51	0.04	-2.75	0.28
28	Me	*m,p*-di-Me-phenyl	H	-2.04	-2.22	0.18	-1.89	-0.15
29	Me	1-naphthyl	6-Me	-0.94	-1.04	0.10	-1.13	0.19
30	Me	1-naphthyl	7-OMe	-0.90	-0.95	0.05	-0.39	-0.51
31	Me	1-naphthyl	6-Br	-0.90	-1.00	0.10	-1.15	0.25
32[e]	Me	1-naphthyl	H	-1.47	-1.43	-0.04	-1.61	0.14
33(R)[f]	Me	1-naphthyl	H	-1.01[m]	-1.01	0.00	-0.85	-0.16
33(S)[f]	Me	1-naphthyl	H	-1.01[m]	-1.06	0.05	-1.14	0.13
34[g]	Me	1-naphthyl	H	-1.67	-1.74	0.07	-2.04	0.37
35[h]	Me	1-naphthyl	H	-2.48	-2.22	-0.26	-2.13	-0.35
36	H	1-naphthyl	6-Me	-0.44	-0.89	0.45	-0.53	0.09
37	H	1-naphthyl	5-F	-1.44	-1.64	0.20	-1.50	0.06
38	H	1-naphthyl	5-Br	-2.17	-1.74	-0.43	-1.55	-0.62
39	H	1-naphthyl	5-OH	-1.74	-1.85	0.11	-1.55	-0.19
(+)-40[f]	H	1-naphthyl	H	-1.95	-1.57	-0.38	-1.92	-0.03
(-)-41[f]	H	1-naphthyl	H	-1.42	-1.32	-0.10	-1.18	-0.24

Compound Designation	R_1	R_2	R_3	pK_i (obsd.)	unprotonated		protonated	
					pK_i (calcd.)	Residual	pK_i (calcd.)	Residual
42(R)[i]	H	1-naphthyl	H	-1.99[m]	-1.74	-0.25	-1.99	0.00
42(S)[i]	H	1-naphthyl	H	-1.99[m]	-1.84	-0.15	-1.90	-0.09
43	Cl	1-naphthyl	H	-0.90	-1.36	0.46	-1.26	0.36
44	H	4-Me-1-naphthyl	H	-0.35	-0.33	-0.02	-0.43	0.08
45	Me	4-Me-1-naphthyl	H	-0.67	-0.63	-0.04	-0.97	0.30
46	H	4-OMe-1-naphthyl	H	-0.04	-0.18	0.14	-0.60	0.56
47	Me	4-OMe-1-naphthyl	H	-1.64	-1.64	-0.00	-1.15	-0.49
48	H	4-OH-1-naphthyl	H	-0.43	-0.53	0.10	-0.62	0.19
49	Me	4-CN-1-naphthyl	H	-1.07	-1.05	-0.02	-1.03	-0.04
50	Me	4-Br-1-naphthyl	H	-0.74	-0.92	0.18	-1.04	0.30
51	Me	2-naphthyl	H	-2.01	-2.28	0.27	-2.11	0.10
52	H	2-naphthyl	H	-1.67	-1.54	-0.13	-1.48	-0.19
53	Me	2-quinolinyl	H	-2.42	-2.15	-0.27	-2.06	-0.36
54	Me	4-quinolinyl	H	-2.35	-2.25	-0.10	-1.97	-0.38
55	Me	5-quinolinyl	H	-2.82	-2.38	-0.44	-2.24	-0.58
56	Me	6-quinolinyl	H	-2.60	-2.50	-0.10	-2.75	0.15
57	H	6-quinolinyl	H	-2.59	-2.55	-0.04	-2.49	-0.10
58	Me	7-quinolinyl	H	-2.15	-2.26	0.11	-2.63	0.48
59	Me	8-quinolinyl	H	-2.34	-1.94	-0.40	-1.97	-0.37
60	Me	2-benzofuryl	H	-2.52	-2.44	-0.08	-2.36	-0.16
61	Me	3-benzofuryl	H	-1.94	-1.81	-0.13	-2.08	0.14
62	H	4-benzofuryl	H	-1.28	-1.54	0.26	-1.37	0.09
63	Me	5-benzofuryl	H	-2.45	-2.58	0.13	-2.80	0.35
64	H	5-benzofuryl	H	-2.04	-2.69	0.65	-2.31	0.27
65	H	6-benzofuryl	H	-2.38	-2.34	-0.04	-2.13	-0.25
66	Me	7-benzofuryl	H	-1.75	-2.47	0.72	-2.02	0.27
67	H	9-anthracenyl	H	-3.37	-3.32	-0.05	-3.43	0.06
68	H	1,2,3,4-H_4-naphthyl	H	-1.48	-1.42	-0.06	-1.51	0.03
69[c]	Me	*p*-OMe-phenyl	H	-2.74	-2.93	0.19	-2.79	0.05
70(R)[j]	Me	*p*-OMe-phenyl	H	-2.59	-2.64	0.05	-2.50	-0.09
71[c]	H	*p*-OMe-phenyl	H	-0.88	-0.79	-0.09	-0.76	-0.12
72[j]	Me	1-naphthyl	H	-0.71	-0.60	-0.11	-0.80	0.09
73[c]	Me	1-naphthyl	H	-0.63	-0.52	-0.11	-0.58	-0.05
74[k]	H	1-naphthyl	H	-0.72	-0.64	-0.08	-0.80	0.08

a) [2-(1,4-di-Me-piperazinyl)]methyl instead of 2-(4-morpholinyl)ethyl for the N1 side chain.
b) [3-(4-Me-morpholinyl)]methyl instead of 2-(4-morpholinyl)ethyl for the N1 side chain.
c) [2-(1-Me-piperidinyl)]methyl instead of 2-(4-morpholinyl)ethyl for the N1 side chain.
d) 2-[4-(1-thiomorpholinyl)]ethyl instead of 2-(4-morpholinyl)ethyl for the N1 side chain.
e) 2-(1-piperidinyl)ethyl instead of 2-(4-morpholinyl)ethyl for the N1 side chain.
f) 1-Me-2-(4-morpholinyl)ethyl instead of 2-(4-morpholinyl)ethyl for the N1 side chain.
g) 2-[4-(2-Me-morpholinyl)]ethyl instead of 2-(4-morpholinyl)ethyl for the N1 side chain.
h) 2-[4-(3-Me-morpholinyl)]ethyl instead of 2-(4-morpholinyl)ethyl for the N1 side chain.
i) 2-Me-2-(4-morpholinyl)ethyl instead of 2-(4-morpholinyl)ethyl for the N1 side chain.
j) [2-(1-Me-pyrrolidinyl)]methyl instead of 2-(4-morpholinyl)ethyl for the N1 side chain.
k) (2-piperidinyl)methyl) instead of 2-(4-morpholinyl)ethyl for the N1 side chain.
l) Data are not available since these compounds are used as the test-set compounds.
m) Reported as racemate, but separately treated in CoMFA models.

Figure 1. Structures and pK_i values of AAIs used as the training set to construct CoMFA model 2. The pK_i is defined as $pK_i = -\log K_i$, where K_i is in nM.

Chart 1

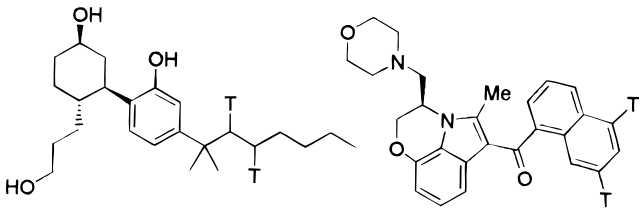

[^{3}H]CP-55940 [^{3}H]WIN-55212-2

assays.[2−5,7] These observations indicate that the mechanism of action of the AAIs involves binding to the CB_1 cannabinoid receptor and inducing a signal transduction response.

The finding that compounds such as the AAIs, although structurally distinct from the cannabinoids, can elicit a cannabimimetic response is intriguing. Surprisingly, the number of published studies of structure−activity relationships (SARs) on the AAIs has been sparse compared with the proliferation of SAR work on the cannabinoids. Bell et al.[1] initially reported a SAR study of the in vitro cyclooxygenase inhibitory potencies of pravadoline and its analogues. In their work, the importance of the N1 side chain, the C2 substituent, and the C3 aroyl group to block prostaglandin synthesis was demonstrated. D'Ambra and co-workers[2] reported that those pravadoline analogues that are conformationally constrained around the N1 side chain show decreased activity to inhibit prostaglandin synthesis in vitro and enhanced activity to inhibit mouse vas deferens contractions. In a recent extensive study by Eissenstat et al.[8a] on AAIs as CB_1 cannabinoid receptor agonists, the following key SAR elements were emphasized: (1) the aminoalkyl side chain at N1, (2) the lipophilic aroyl group at C3, and (3) the heterocyclic indole ring.

In the present study, we apply the method of comparative molecular field analysis[9] (CoMFA) to develop a 3D-QSAR model that correlates variations in the AAI structures with variations in their observed CB_1 cannabinoid receptor binding activities. CoMFA has established itself as a versatile and powerful tool in rational drug design[10] and related applications.[11] CoMFA systematically samples the steric and electrostatic fields surrounding a set of ligands and constructs a 3D-QSAR model by correlating these 3D steric and electrostatic fields with the corresponding observed binding affinities. In a recent study,[12] we successfully developed a CoMFA model for the AC and ACD nonclassical cannabinoids. We now present two distinct CoMFA models based on separate sets of receptor binding data on AAI analogues in which two different radioligands to the CB_1 cannabinoid receptor were competitively displaced: the cannabinoid radioligand [^{3}H]CP-55940 (Chart 1) and the AAI radioligand [^{3}H]WIN-55212-2.[8] Comparison of the CoMFA contour plots from each model allowed us to examine likely regions of structural homology between the cannabinoids and AAIs with respect to CB_1 cannabinoid receptor binding. In addition, the model derived from AAI displacement of [^{3}H]-CP-55940 (CoMFA model 1) was used to predict the K_i values of the AAIs displacing [^{3}H]WIN-55212-2 (CoMFA model 2) which were then correlated with their corresponding experimental K_i values. A strong correlation would imply that the AAIs and the classical cannabinoids interact with common sites of interaction within the CB_1 cannabinoid receptor. The derivation and refinement of these models also enabled us to examine aspects of the CoMFA methodology.

Methods

All calculations in this study were carried out using the Sybyl V6.3 molecular modeling program[13] implemented on a Silicon Graphics R4000 Indigo Elan or R5000 Indy workstation.

CB_1 Cannabinoid Receptor and Adenylate Cyclase Assays. Radioligand binding assays using [^{3}H]CP-55940 and rat forebrain washed P2 membranes were performed and analyzed exactly as previously described.[14] Adenylate cyclase activity was determined in purified N18TG2 neuroblastoma membranes as previously described.[15] Secretin (900 nM) was present as the hormonal stimulator, and rolipram (100 μM) was present as the phosphodiesterase inhibitor. The AAI compounds were synthesized at Sterling Winthrop Research Institute. Compounds were stored as stock solutions (100 mM) in dimethyl sulfoxide at −20 °C and subsequently diluted in a buffer containing 50 mM Tris-HCl, pH 7.4, 1 mM Tris-EDTA, 3 mM $MgCl_2$, and 0.15 mg/mL fatty acid-deficient bovine serum albumin prior to assay. [^{3}H]CP-55940 was purchased from New England Nuclear. Data from multiple experiments (a minimum of three) were averaged and analyzed to determine the IC_{50} (binding competition) and EC_{50} (adenylate cyclase) values using the GraphPAD Inplot program. K_i values were calculated as previously described.[14]

Separate sets of binding data for two series of AAIs were used to develop a common pharmacophore from which two separate CoMFA models (model 1 and model 2) were derived. CoMFA model 1 was constructed from K_i values for 14 AAI compounds (Figure 2) based on the in vitro heterologous displacement of [^{3}H]CP-55940 binding to CB_1 cannabinoid receptors in rat brain membranes (Figure 3; Table 1). CoMFA model 2 was based on the reported IC_{50} data for 64 selected AAI derivatives whose binding affinity was measured by displacement of [^{3}H]WIN-55212-2 as the radioligand.[8] These IC_{50} values were converted to the corresponding K_i values using the Cheng−Prusoff equation.[16] As seen in Figure 1, the structures of these compounds differ from one another mainly with respect to substitution at three different positions on the indole ring: the C3 aroyl moiety, the C2 position, and the C4−C7 positions.

Molecular Models and Structural Alignment. Initial structures for the AAIs were built based on the recently published X-ray crystallographic structure of (1-naphthyl)[6-isothiocyanato-1-[2-(4-morpholinyl)ethyl]-1*H*-indol-3-yl]methanone, the only compound in this series for which 3D structural data were available in the literature.[17] This crystal structure was modified as required to build each AAI molecule using the molecular fragments library provided within Sybyl, after which each AAI structure was energy-minimized using the Tripos force field with a distance-dependent dielectric function and a convergence criterion of 0.001 kcal/mol·Å energy difference between successive iterations. The partial atomic charges required to calculate the electrostatic interactions were assigned based on the Gasteiger−Marsili formalism.[18] To identify a low-energy conformation, systematic searching of the torsion angles around the C3−C(=O) and C(=O)−C1′ bonds in 15° increments was carried out while holding the torsion angles of the N1 side chain fixed as in the crystal structure.[17] The reasons for holding the torsion angles of the N1 side chain fixed are 3-fold: (1) the N1 ethylamino side chain (as in morpholinoethyl) is invariant among the AAIs in this study; (2) the above X-ray crystallographic structure is in good agreement with other studies,[1,8b] in which the preferred positioning of the N1 morpholine side chain for mouse vas deferens relaxation activity is in the lower right quadrant with the C3 aroyl group in the upper right quadrant, beneath the

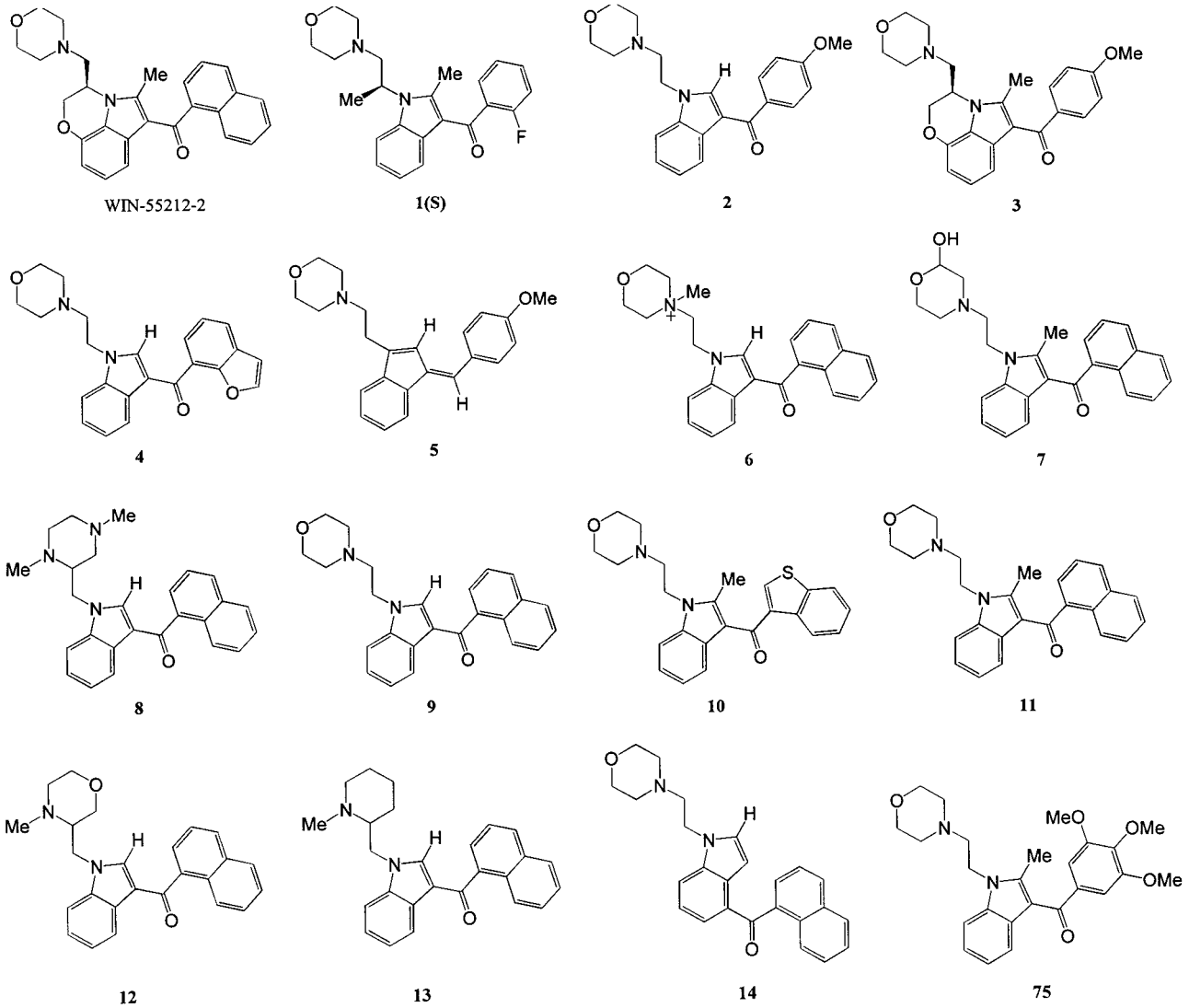

Figure 2. Structures of 14 AAIs used as the training set to construct CoMFA model 1. Also shown are compounds **14** and **75** which belonged to the test set for CoMFA model 1.

indole ring plane;[2] and (3) fixing the torsional angles of the N1 side chain renders the conformational problem more tractable from a computational perspective.

Based on the measured pK_a's of 4.5−6.0 for pravadoline and its analogues,[2] it was deduced that the morpholine nitrogen of AAI would exist largely unprotonated at physiological pH. However, it is possible that there exists within the receptor binding site a specific residue capable of protonating the morpholine nitrogen. Moreover, the pK_a of morpholine itself is moderately high (8.49).[19] Accordingly, the training set compounds for CoMFA model 1 and CoMFA model 2 were modeled in two forms: (i) one form in which the morpholine nitrogen is unprotonated except compound 6 whose morpholine nitrogen is quaternary (CoMFA model $1_{unprotonated}$ and CoMFA model $2_{unprotonated}$) and (ii) a second form in which the morpholine nitrogen is protonated to yield a +1 charged species (CoMFA model $1_{protonated}$ and CoMFA model $2_{protonated}$). If the AAI contains another N-containing heterocyclic moiety besides morpholine within the N1 side chain, the nitrogen at the γ position from the N1 was usually protonated. For other basic nitrogen sites existing in some of the AAIs, the decision whether or not to protonate was based on whichever case gave the better CoMFA model in terms of the statistical parameters.

The goal of the present study was to develop a 3D-QSAR model for binding of the subject AAIs to the CB_1 cannabinoid receptor. It was also intended to address some questions relating to the CoMFA methodology itself. Consequently, several variations in the development of CoMFA model 1 were attempted, specifically: (1) different alignment schemes for the molecules, (2) different methods (i.e., Gasteiger−Marsili, AM1) for generating the partial atomic charges, and (3) randomization of activities. Among these various protocols, the one found statistically most valid for CoMFA model 1 was applied for development of CoMFA model 2.

For each CoMFA model, the template molecule for alignment was selected among those highly potent AAIs in each data set that contain the key structural features of the compounds comprising the model. With this aim in mind, the prototypical AAI ligand WIN-55212-2 was selected among the 14 AAIs comprising CoMFA model 1 and compound **46** (Figure 1) was selected among the 64 AAIs[8] comprising CoMFA model 2. All compounds in their respective data sets were aligned onto the template molecule by root-mean-square (rms) fitting onto three common atoms (refer to Results and Discussion for details).

Applying standard CoMFA procedures, the training set compounds were placed sequentially inside a 3D cubic lattice divided into a grid with a 2-Å spacing. The steric (van der Waals) and electrostatic (Coulombic) energies were then calculated between the atoms of each molecule and a probe atom, represented by a sp^3 carbon with a +1 charge, which is placed at each grid point. Calculated energies above 30 kcal/mol were set to this value.

PLS-QSAR. An initial partial least-squares (PLS)[20] analysis was performed using the "leave-one-out" cross-validation procedure[21] to determine the optimum number of principal

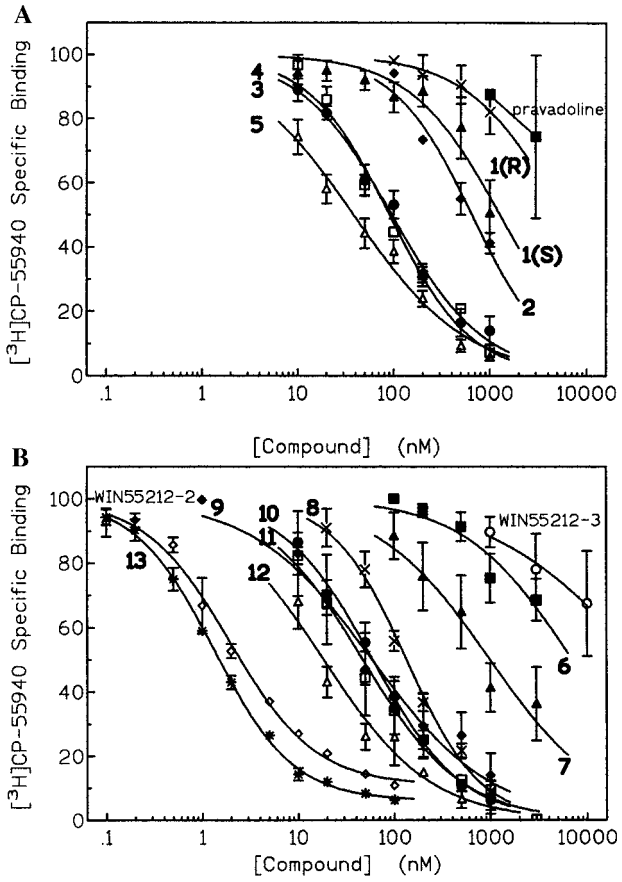

Figure 3. Displacement of [^{3}H]CP-55940 from rat brain CB_1 cannabinoid receptors by a series of AAI compounds. Radioligand binding assays were performed by heterologous displacement with a series of (A) *p*-methoxyphenyl or *o*-fluorophenyl and (B) naphthyl or bicyclic ring AAI derivatives. Compounds were tested over a range of concentrations such that K_i values could be determined (Table 1). Data points are the mean ± SEM of values from ≥3 individual experiments. For A: ■, pravadoline; ×, **1**(*R*); ▲, **1**(*S*); ◆, **2**; ●, **3**; □, **4**; △, **5**. For B: ■, **6**; ▲, **7**; ×, **8**; ◆, **9**; ●, **10**; □, **11**; △, **12**; *, **13**; ◇, WIN-55212-2; ○, WIN-55212-3.

components needed for subsequent analysis of the data. The PLS analysis was then repeated without cross-validation using the optimum number of components corresponding to that which yielded the smallest standard error of prediction or the highest cross-validated r^2 (r_{CV}^2) value. This final analysis yielded a predictive model and associated conventional r^2 values, from which the CoMFA coefficient contour plots for the steric and electrostatic potentials could be generated.

Results and Discussion

AAI Compounds as Agonists at the CB_1 Cannabinoid Receptor. The CB_1 cannabinoid receptor was originally identified and pharmacologically characterized using [^{3}H]CP-55940, a bicyclic cannabinoid agonist radioligand, and a series of bicyclic and tricyclic cannabinoid derivatives.[14,22,23] AAI analgesics were shown to interact with the CB_1 cannabinoid receptor in studies of competitive displacement of [^{3}H]WIN-55212-2 by cannabinoid ligands[6] and competitive displacement of [^{3}H]CP-55940 by AAI ligands.[5] Isothiocyanate derivatives of two AAIs (compounds **9** and **11**) exhibited affinity for the cannabinoid receptor.[17] After covalent binding of one such derivative to the CB_1 cannabinoid receptor, the binding of [^{3}H]CP-55940 was precluded.[17] These studies indicate that the two classes of ligands may occupy mutually exclusive regions within the receptor space. To more fully characterize the SAR of AAI ligands for the cannabinoid binding sites, a series of compounds having a wide range of ability to displace [^{3}H]WIN-55212-2 were tested for their ability to competitively displace [^{3}H]CP-55940 (Figure 3). The slope factors for competitive displacement were close to 1 for each of these ligands, suggesting single-site displacement of [^{3}H]CP-55940. The two most potent compounds, WIN-55212-2 and **13**, produced a competition curve that failed to fully displace [^{3}H]CP-55940, leaving 10% and 5%, respectively, of the specifically bound [^{3}H]-CP-55940 as defined by displacement of the radioligand by 200 nM desacetyllevonantradol. This may indicate the presence of a minor subpopulation of the CB_1 cannabinoid receptor that binds cannabinoid ligands preferentially. It should be noted that error in the data was particularly large at concentrations exceeding 1 μM, thereby limiting the extent of the log dose−response curves for low-affinity ligands. This variability is probably a result of the hydrophobic nature of these compounds and their poor aqueous solubility at high concentrations.

CB_1 cannabinoid receptors in N18TG2 cells are coupled to G_i which mediates inhibition of adenylate cyclase activity. To demonstrate that the potency as an agonist is related to the affinity of the AAI agonist for the CB_1 cannabinoid receptor, compounds having a wide range of affinities were tested for their ability to inhibit adenylate cyclase (Figure 4A). The maximal inhibition achieved by the potent compounds was equivalent to the maximal response obtained with the cannabinoid agonist desacetyllevonantradol (data not shown), suggesting that these AAI compounds are full agonists in this preparation. The slope factor for the log dose−response curves was close to 1. Thus, there was no evidence of cooperativity or multiple receptor involvement in the response. There was excellent correlation between the affinity for the [^{3}H]CP-55940 binding sites and the ability to behave as an agonist ligand for these five compounds (Figure 4B). Enantioselectivity was noted for the WIN-55212-2 and WIN-55212-3 pair.

Building the CoMFA Models. Of several variations in the alignment scheme considered, the best results were obtained by superimposing three common atoms which yielded not only a reasonably good overlap of the putative biologically relevant pharmacophore elements but also statistically significant 3D-QSAR models from CoMFA. The atoms selected are as follows: for the unprotonated models, the indole N1 atom, the C_α or H_α atom on C2, and the O atom of the C3 carbonyl; and for the protonated models, the C_α atom of the N1 side chain, the indole C3 atom, and the C1′ atom on the C3 carbonyl atom. It was found that CoMFA model $1_{protonated}$ improved slightly when partial atomic charges were derived from Gasteiger-Marsili ($r_{CV}^2 = 0.58$) rather than from AM1 ($r_{CV}^2 = 0.52$). Other workers have reported improved results with AM1-derived charges over other methods.[24] This sensitivity to the choice of method for calculating partial charges, although minimal in the present application, may be significant in some cases.

Both CoMFA models 1 and 2 required six principal

Table 1. Observed versus CoMFA-Predicted pK_i Values for the Training Set of 14 Compounds (CoMFA Model 1)

compd	pK_i (obsd)	pK_i (pred), unprotonated	residual	pK_i (pred), protonated	residual
WIN-55212-2	−0.04	−0.16	0.12	−0.05	0.01
1 (*S*)	−2.95	−2.98	0.03	−2.95	0.00
2	−2.55	−2.56	0.01	−2.56	0.01
3	−1.74	−1.67	−0.07	−1.72	−0.02
4	−1.74	−1.75	0.01	−1.76	0.02
5	−1.32	−1.36	0.04	−1.31	−0.01
6	−3.41	−3.40	−0.01	−3.43	0.02
7	−2.65	−2.66	0.01	−2.67	0.02
8	−1.96	−2.00	0.04	−1.94	−0.02
9	−1.68	−1.71	0.03	−1.69	0.01
10	−1.48	−1.49	0.01	−1.46	−0.02
11	−1.45	−1.35	−0.10	−1.45	0.00
12	−1.03	−0.94	−0.09	−0.98	−0.05
13	0.12	0.14	−0.02	0.09	0.03

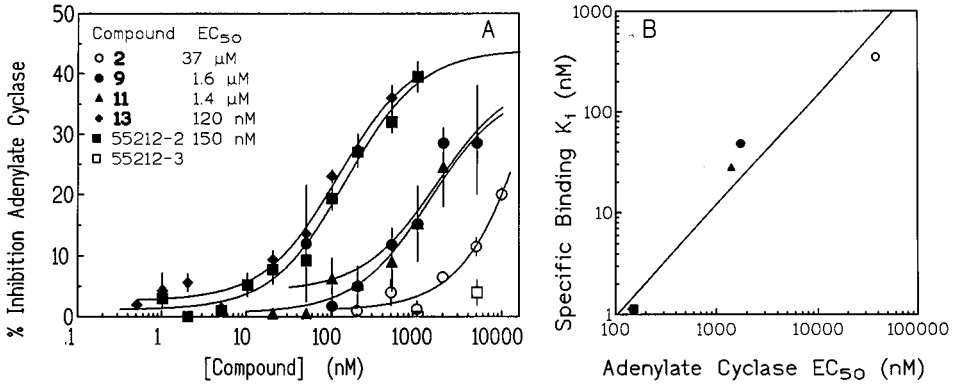

Figure 4. Ability of a series of AAI derivatives to behave as agonists to inhibit hormone-stimulated adenylate cyclase activity. (A) Compounds were included in the assay over a range of concentrations, and the data for each individual experiment were calculated as the percent inhibition of secretin-stimulated activity. Data points are the mean ± SEM of 3 individual experiments for each compound, and the EC_{50} was determined as a parameter of the curve. (B) Correlation of EC_{50} values for inhibition of adenylate cyclase with K_i values describing affinity for the CB_1 cannabinoid receptor for the compounds in panel A.

Table 2. Summary of Statistical Analysis and Field Contributions for CoMFA Models 1 and 2

	CoMFA model l		CoMFA model 2	
	unprotonated	protonated	unprotonated	protonated
	Statistical Parameters			
r^2	0.997	1.000	0.915	0.905
standard error of estimate	0.078	0.028	0.271	0.286
F	354	2763	102	90
P	<0.001	<0.001	<0.001	<0.001
r_{CV}^2	0.155	0.624	0.563	0.592
	Field Contributions			
steric	54%	81%	71%	80%
electrostatic	46%	19%	29%	20%

components (PCs) to explain the variance in binding affinity to CB_1 cannabinoid receptors in rat brain membranes. Values of pertinent statistical parameters for both CoMFA models 1 and 2, along with the individual contributions from the steric−electrostatic fields, are shown in Table 2. The corresponding experimental and calculated pK_i values in units of nM from CoMFA models 1 and 2 are listed in Table 1 and Figure 1, respectively. Although CoMFA model $1_{unprotonated}$ yielded an exceptionally good r^2 value of 0.997, its r_{CV}^2 value of 0.155 failed to surpass the generally accepted criterion for statistical validity (i.e., $r_{CV}^2 \geq 0.5$). The three remaining CoMFA models all exceeded this criterion, and each exhibited a strong linear correlation between the corresponding CoMFA-calculated and experimental values of the CB_1 cannabinoid receptor binding affinity (Figure 5). Based on comparison of their statistical parameters alone (Table 2), it is difficult to conclude definitively from the respective CoMFA models whether the training set compounds are more appropriately represented in their protonated or unprotonated form. For CoMFA model 1, the protonated form is clearly superior to the unprotonated form from the standpoint of every statistical measure listed in Table 2. One might infer that at least the AAIs belonging to this training set bind at the receptor as protonated species. For CoMFA model 2, however, there is little to choose between the protonated and unprotonated forms in terms of the quality of their respective statistical parameters. The larger size of the training set for CoMFA model 2 compared with CoMFA model 1 (64 vs 14 AAIs, respectively) strengthens the statistical robustness of the former and, hence, our confidence in its statistical validity. Consequently, no conclusive statement can be made as to the likely state of protonation

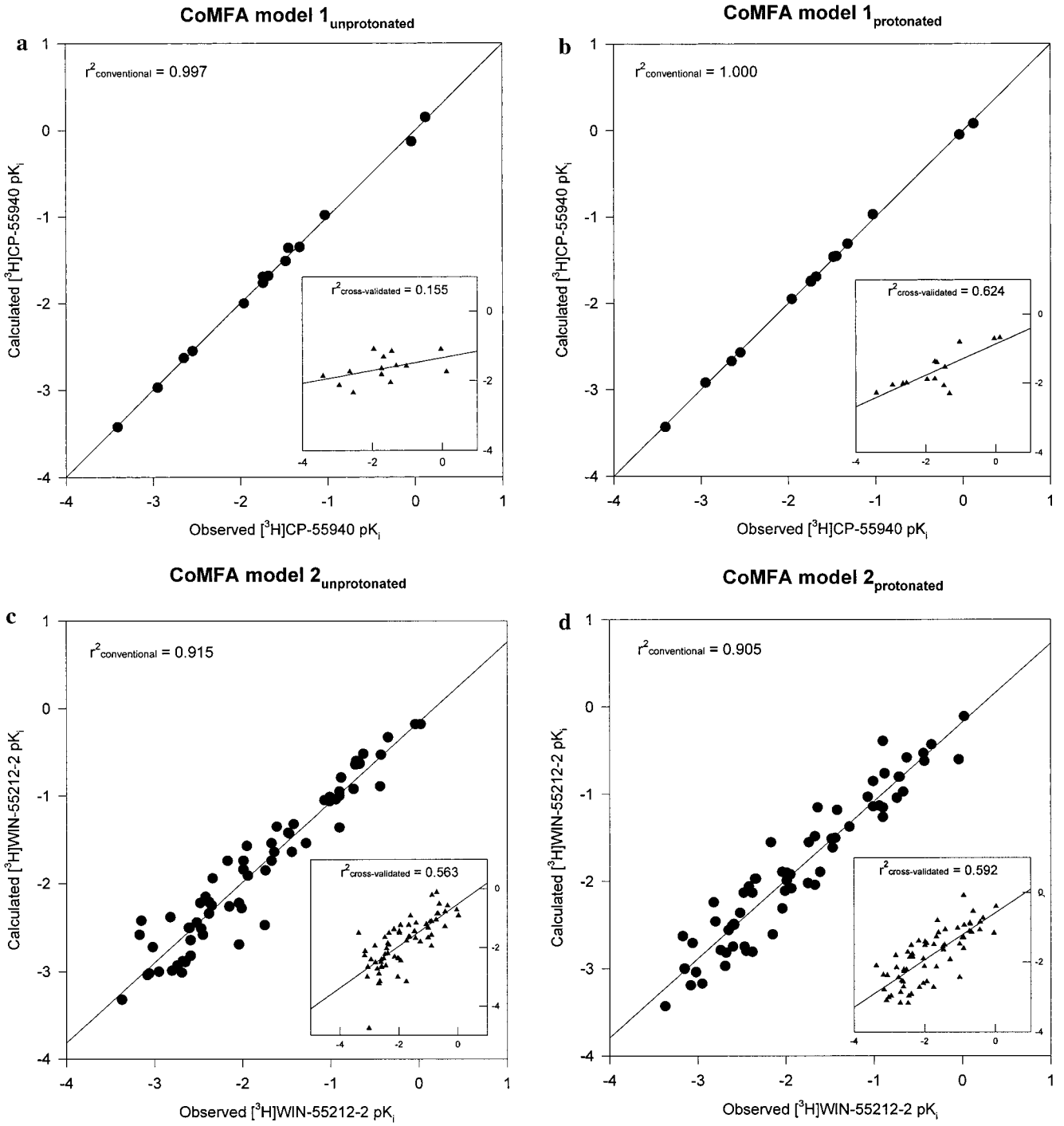

Figure 5. Observed versus CoMFA-predicted pK_i values for the training set of 14 AAI compounds in CoMFA model 1: (a) unprotonated, (b) protonated. Observed versus CoMFA-predicted pK_i values for the training set of 64 AAI compounds in CoMFA model 2: (c) unprotonated, (d) protonated.

(i.e., neutral versus +1 charged) of these AAIs as receptor-bound species.

To address the possibility that CoMFA models 1 and 2 might be the result of chance correlation, a separate CoMFA model was constructed for the same training set of compounds but whose pK_i values were deliberately randomized. The average r_{CV}^2 value obtained from 10 of these randomized data sets was −0.17 for CoMFA model $1_{protonated}$ and 0.08 for CoMFA model $2_{unprotonated}$. These results concur with our assertion that the present CoMFA models are unlikely the result of chance correlation.

Prediction of Binding Affinity for the Test Compounds. The CB_1 cannabinoid receptor binding affinity of the test compounds was calculated to evaluate the predictive ability of both CoMFA models beyond their respective training sets. The test compounds selected were pravadoline and compounds **14** and **75** for CoMFA model 1 and pravadoline and compounds **2**, **4**, **9**, **11**, and **12** for CoMFA model 2. The range of binding affinities for the latter set of compounds was 3.0 log units (viz., the absence of a pK_i value for pravadoline precludes stating a range for the former set of compounds). Table 3 lists the observed and corresponding CoMFA-predicted

Table 3. Observed versus CoMFA-Predicted pK_i Values for Test Set Compounds

	CoMFA model 1			CoMFA model 2		
		pK_i (pred)			pK_i (pred)	
compd	pK_i (obsd)	unprotonated	protonated	pK_i (obsd)	unprotonated	protonated
pravadoline		−2.83	−2.92	−3.40	−3.26	−3.22
2	−2.55			−2.49	−2.02	−2.01
4	−1.74			−1.15	−1.51	−1.18
9	−1.68			−0.78	−1.54	−1.50
11	−1.45			−1.18	−1.70	−1.88
12	−1.03			−0.38	−0.48	−0.36
14[a]	−2.37	−2.35	−2.21			
75	−2.57	−2.61	−2.54			

[a] C6, carbonyl C, and C1′ on the C3 aroyl group of compound **14** were aligned onto C3, carbonyl C, and C1′, respectively, on the C3 aroyl group of WIN-55212-2.

pK_i values of the test compounds according to each CoMFA model. The pK_i value of compound **14** was predicted by CoMFA model $1_{unprotonated}$ and CoMFA model $1_{protonated}$ to within 0.02 and 0.16 log unit, respectively, of its experimental value. The pK_i value of compound **75** was predicted by CoMFA model $1_{unprotonated}$ and CoMFA model $1_{protonated}$ to within 0.04 and 0.03 log unit, respectively, of its experimental value. Although an experimental pK_i value for pravadoline is not available due to lack of sufficient data points to calculate it, the predicted pK_i values of −2.83 from CoMFA model $1_{unprotonated}$ and −2.92 from CoMFA model $1_{protonated}$ appear reasonable and consistent with the biological data in Figure 3 which demonstrate that pravadoline displaces [^{3}H]CP-55940 in the micromolar range. The structurally related compound **2** (pK_i = −2.55) listed in Table 1 was predicted as more potent than pravadoline: In general, the pK_i values are more negative for compounds with a methyl substituent at C2 than for compounds without any substituent (see Figure 1).

For CoMFA model $2_{unprotonated}$ and CoMFA model $2_{protonated}$, the activities of the test compounds were predicted to within 0.76 and 0.72 log unit, respectively, of their corresponding experimental values regardless of whether they are high-affinity or low-affinity analogues (Table 3). For CoMFA model $2_{unprotonated}$ and CoMFA model $2_{protonated}$, the residual standard deviation was 0.39 and 0.36 log unit, respectively, across a range of 3.0 log units.

CoMFA Contour Maps. The individual contributions from the steric−electrostatic fields were 51%/49% and 80%/20%, respectively, for CoMFA model $1_{unprotonated}$ and CoMFA model $1_{protonated}$ and 71%/29% and 80%/20%, respectively, for CoMFA model $2_{unprotonated}$ and CoMFA model $2_{protonated}$. These field contributions indicate that the variation in binding affinity among the AAIs is dominated by steric interactions at the receptor site. This result is consistent with the recognized importance of the hydrophobic components of the classical cannabinoids (i.e., the C3 side chain)[14] and of the AAIs (i.e., the C3 aroyl moiety)[8] for cannabimimetic activity.

The steric−electrostatic StDev*Coeff color contour maps for CoMFA model 1 (Figure 6) and model 2 (Figure 7) depict regions around the molecules where enhanced CB_1 cannabinoid receptor binding affinity is associated with increasing (green) and decreasing (yellow) steric bulk and with increasing (red) and decreasing (blue) negative charge. The CoMFA steric and electrostatic fields are consistent with the known SAR for AAIs. For example, the green contour in the region around the C3 aroyl moiety for CoMFA model $1_{protonated}$ (Figure 6, right) indicates that the presence of bulky groups, such as the bicyclic substitution at the C3 carbonyl found in compounds WIN55212-2 and **9**, is expected to enhance binding affinity, compared with the corresponding compounds with monocyclic substitution found in compounds **2** and **3**. Consistent with the presence of both green and yellow contours closely surrounding the heterocyclic ring in the N1 side chain (see Figure 6, right), enhanced binding affinity is shown for compound **13** in which a methyl group on the pyrolidinyl ring appears close to the green contour, while diminished binding is found for compound **8** in which one of the methyl groups on the piperazinyl ring appears close to the yellow contour. The rather large blue contour near the morpholine moiety emphasizes the importance of the basicity of this structural element for binding.

For CoMFA model 2 (Figure 7), the StDev*Coeff contour map for the steric−electrostatic contributions exhibits a yellow contour in the region surrounding C2′ and C3′ of the naphthyl moiety to indicate a sterically forbidden region. Consistent with this conclusion, substitution in this region is expected to diminish binding as exemplified by compounds **24**, **57**, **60**, and **64**. On the aroyl end of the AAI molecule, the green contour indicates that the presence of a lipophilic group promotes increased binding inside a presumed large hydrophobic pocket within the receptor cavity. Such is the case in the present training set when, for example, the naphthyl moiety (compounds **45** and **47**) replaces the substituted phenyl moiety (pravadoline and compound **23**, respectively). In addition, the blue contour surrounding C4′ of the naphthyl moiety is consistent with the enhanced CB_1 cannabinoid receptor binding affinity associated with the presence of a methoxy (compound **46**) or a bromo (compound **50**) substituent at this position.

The K_i values for the AAI compounds comprising CoMFA model 1 were measured by competitive displacement of the cannabinoid ligand CP-55940 for the CB_1 cannabinoid receptor; hence it might be expected that CoMFA model 1 would provide some information on both the cannabinoid and CB_1 cannabinoid receptor AAI binding site. Similarly, the K_i values for the AAI compounds comprising CoMFA model 2 were measured by competitive displacement of the AAI ligand WIN-55212-2 for the CB_1 cannabinoid receptor. This suggests that CoMFA model 2 would provide information more exclusively on the AAI binding site within the CB_1 cannabinoid receptor. As points of commonality, both

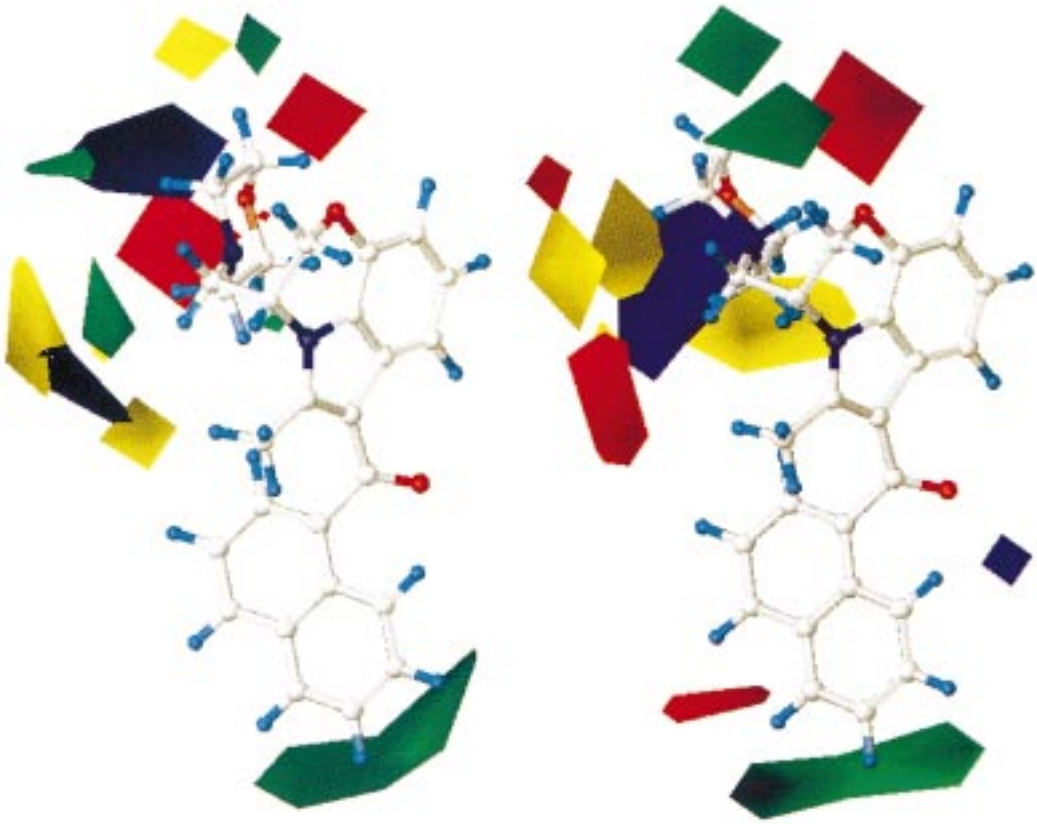

Figure 6. CoMFA steric−electrostatic contour plots for CoMFA model 1 with WIN-55212-2 inserted as a reference molecule: (left) unprotonated and (right) protonated. Colored-coded contours depict regions around the AAI molecules where enhanced binding is associated with increasing (green) and decreasing (yellow) steric bulk and with increasing (red) and decreasing (blue) negative charge. Stereoviews are available upon request.

CoMFA StDev*Coeff contour maps reveal that the region close to the C6′ and C7′ sides of the C3 naphthyl group is sterically favored. This observation is consistent with the fact that steric interactions predominate in both models. The similarity of the two steric−electrostatic contour maps (Figures 6 and 7) suggests that the classical cannabinoids and AAIs, although structurally quite different, occupy substantial regions of the CB_1 cannabinoid receptor binding pocket in common. However, the differences support the suggestion that AAIs and cannabinoids differ in at least one binding interaction within the CB_1 cannabinoid receptor. A critical lysine is required for interaction with the cannabinoid ligand in the CB_1 cannabinoid receptor, but it is apparently not important for interaction with AAI ligands.[25]

Correlation of Binding Data. There are seven compounds (compounds **2**, **4**, **8**, **9**, **11**, **12**, and **13**) in the two data sets for which binding data have been measured in both assay systems. Except for compound **13**, values of the AAI binding affinity are consistently lower for [^{3}H]CP-55940 than for [^{3}H]WIN-55212-2, and this may reflect differences in the assay conditions. A strong positive correlation of binding affinities determined by the two displacement procedures suggests a common binding mode for the cannabinoids and AAIs. The following analysis was carried out to explore this hypothesis. First, CoMFA model $1_{protonated}$ was used to predict the pK_i values of the training set compounds belonging to CoMFA model $2_{protonated}$. This operation was intended to adjust the pK_i values of these training set compounds from what they actually were using the AAI radioligand [^{3}H]WIN-55212-2 to what they would be if the cannabinoid radioligand [^{3}H]CP-55940 was used instead. Then, these predicted values (corresponding to using radioligand [^{3}H]CP-55940) were compared with the corresponding experimental pK_i values (using radioligand [^{3}H]WIN-55212-2) for these compounds to seek a linear correlation.

The best least-squares-fit plot (Figure 8) between the experimental pK_i values for the training set compounds using the AAI radioligand [^{3}H]WIN-55212-2 and the predicted pK_i values for the same compounds using the cannabinoid radioligand [^{3}H]CP-55940 yielded a moderately strong linear correlation (correlation coefficient $r = 0.73$). This moderately strong correlation can be viewed within the context of whether the classical cannabinoids and AAIs interact with the same binding site(s) within the cannabinoid receptor. Although not definitive, the present results suggest at least that the CB_1 cannabinoid receptor binding sites of the classical cannabinoids and AAIs may partly overlap and that the two distinct classes of compounds share some common structural features to allow association with the CB_1 cannabinoid receptor. At the same time, it is clearly possible and highly likely based on structural comparisons that each class of compounds exhibits unique interactions within the receptor. Work is currently underway in our laboratory to compare the AAIs and cannabinoids with respect to similarities and differences in their pharmacophoric elements and spatial features in order to elucidate the essential binding requirements for activation of the CB_1 cannabinoid receptor. At the same time, work is in progress in applying the present

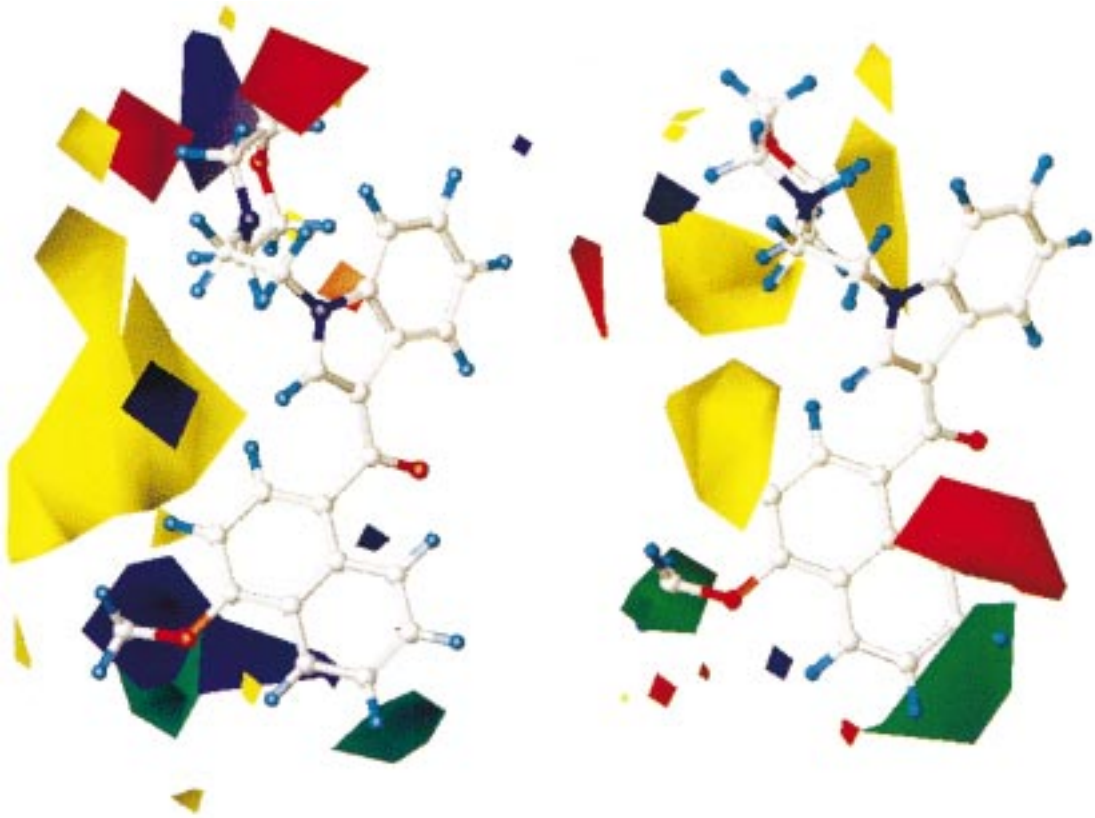

Figure 7. CoMFA steric and electrostatic contour plots for CoMFA model 2 with compound **46** inserted as a reference molecule: (left) unprotonated and (right) protonated. Colored-coded contours depict regions around the AAI molecules where enhanced binding is associated with increasing (green) and decreasing (yellow) steric bulk and with increasing (red) and decreasing (blue) negative charge. Stereoviews are available upon request.

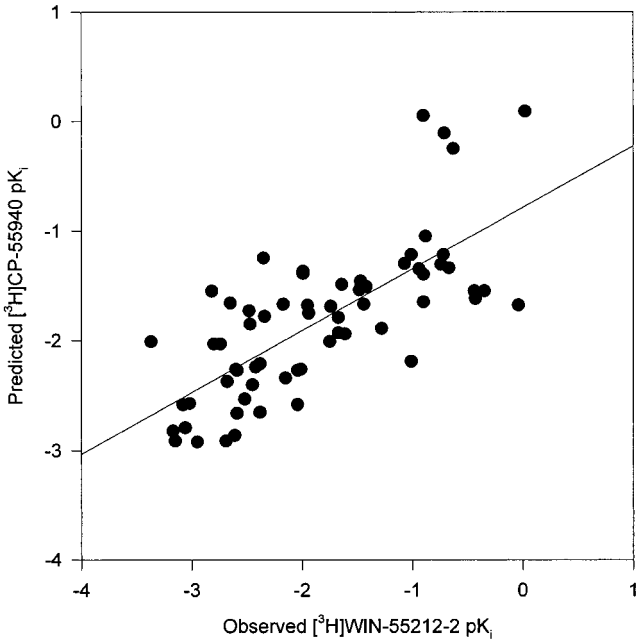

Figure 8. Correlation between pK_i values predicted by CoMFA model $1_{protonated}$ and observed values for the training set compounds in CoMFA model 2.

computational approaches to compare the CB_1 and CB_2 cannabinoid receptors in terms of similarities and differences of their pharmacophoric maps and ligand selectivities. These studies are aimed toward the rational design of highly potent and selective lead compounds for medicinal applications.

Acknowledgment. This research has been funded in part by NIH Grants R01-06312 and K05-00182. The authors thank Gerald Wilken for technical assistance on the adenylate cyclase experiments.

References

(1) Bell, M. R.; D'Ambra, T. E.; Kumar, V.; Eissenstat, M. A.; Herrmann, J. L., Jr.; Wetzel, J. R.; Rosi, D.; Philion, R. E.; Daum, S. J.; Hlasta, D. J.; Kullnig, R. K.; Ackerman, J. H.; Haubrich, D. R.; Luttinger, D. A.; Baizman, E. R.; Miller, M. S.; Ward, S. J. Antinociceptive (Aminoalkyl)indoles. *J. Med. Chem.* **1991**, *34*, 1099−1110.

(2) D'Ambra, T. E.; Estep, K. G.; Bell, M. R.; Eissenstat, M. A.; Josef, K. A.; Ward, S. J.; Haycock, D. A.; Baizman, E. R.; Casiano, F. M.; Beglin, N. C.; Chippari, S. M.; Grego, J. D.; Kullnig, R. K.; Daley, G. T. Conformationally Restrained Analogues of Pravadoline: Nanomolar Potent, Enantioselective, (Aminoalkyl)indole Agonists of the Cannabinoid receptor. *J. Med. Chem.* **1992**, *35*, 124−135.

(3) Haubrich, D. R.; Ward, S. J.; Baizman, E.; Bell, M. R.; Bradford, J.; Ferrari, R.; Miller, M.; Perrone, M.; Pierson, A. K.; Saelens, J. K.; Luttinger, D. Pharmacology of Pravadoline: A New Analgesic Agent. *J. Pharmacol. Exp. Ther.* **1990**, *255*, 511−522.

(4) Ward, S. J.; Mastriani, D.; Casiano, F.; Arnold, R. Pravadoline: Profile in Isolated Tissue Preparations. *J. Pharmacol. Exp. Ther.* **1990**, *255*, 1230−1239.

(5) Ward, S. J.; Baizman, E.; Bell, M.; Childers, S.; D'Ambra, T.; Eissenstat, M.; Estep, K.; Haycock, D.; Howlett, A.; Luttinger, D.; Miller, M.; Pacheco, M. (Aminoalkyl)indoles (AAIs): A New Route to the Cannabinoid Receptor? *NIDA Res. Monogr.* **1990**, *105*, 425−426.

(6) Kuster, J. E.; Stevenson, J. I.; Ward, S. J.; D′Ambra, T. E.; Haycock, D. A. Aminoalkylindole Binding in Rat Cerebellum: Selective Displacement by Natural and Synthetic Cannabinoids. *J. Pharmacol. Exp. Ther.* **1992**, *264*, 1352−1363.

(7) Pacheco, M.; Childers, S. R.; Arnold, R.; Casiano, F.; Ward, S. J. Aminoalkylindoles: Actions on Specific G-Protein-Linked Receptors. *J. Pharmacol. Exp. Ther.* **1990**, *257*, 170−183.

(8) Eissenstat, M. A.; Bell, M. R.; D'Ambra, T. E.; Alexander, E. J.; Daum, S. J.; Ackerman, J. H.; Gruett, M. D.; Kumar, V.; Estep, K. G.; Olefirowicz, E. M.; Wetzel, J. R.; Alexander, M. D.; Weaver, J. D., III; Haycock, D. A.; Luttinger, D. A.; Casiano, F.

M.; Chippari, S. M.; Kuster, J. E.; Stevenson, J. I.; Ward, S. J. Aminoalkylindoles: Structure−Activity Relationships of Novel Cannabinoid Mimetics. *J. Med. Chem.* **1995**, *38*, 3094−3105. (b) D'Ambra, T. E.; Eissenstat, M. A.; Abt, J.; Ackerman, J. H.; Bacon, E. R.; Bell, M. R.; Carabateas, P. M.; Josef, K. A.; Kumar, V.; Weaver, J. D., III; Arnold, R.; Casiano, F. M.; Chippari, S. M.; Haycock, D. A.; Kuster, J. E.; Luttinger, D. A.; Stevenson, J. I.; Ward, S. J.; Hill, W. A.; Khanolkar, A.; Makriyannis, A. C-Attached Aminoalkylindoles: Potent Cannabinoid Mimetics. *Bioorg. Med. Chem. Lett.* **1996**, *6*, 17−22.

(9) Cramer, R. D., III; Patterson, D. E.; Bunce, J. D. Comparative Molecular Field Analysis (CoMFA). 1. Effect of Shape on Binding of Steroids to Carrier Proteins. *J. Med. Chem.* **1988**, *110*, 5959−5967.

(10) Tong, W.; Collantes, E. R.; Chen, Y.; Welsh, W. J. A Comparative Molecular Field Analysis (CoMFA) Study of N-benzylpiperidines as Acetylcholinesterase Inhibitors. *J. Med. Chem.* **1996**, *35*, 124−135. Waller, C. L.; Juma, B. W.; Gray, L. E.; Kelce, W. R. Three-dimensional quantitative structure−activity relationships for androgen receptor ligands. *Toxicol. Appl. Pharmacol.* **1996**, *137*, 219−227.

(11) Collantes, E. R.; Tong, W.; Welsh, W. J.; Zielinski, W. L. Use of Moment of Inertia in Comparative Molecular Field Analysis to model Chromatographic Retention of Nonpolar Solutes. *Anal. Chem.* **1996**, *68*, 2038−2043.

(12) Tong, W.; Collantes, E. R.; Welsh, W. J.; Berglund, B.; Howlett, A. Derivation of a Pharmacophore model for Anandamide Using Constrained Conformational Searching and Comparative Molecular Field Analysis (CoMFA). *J. Med. Chem.* **1998**, *41*, 4207−4215.

(13) Sybyl is a product of Tripos, Inc., St. Louis, MO 63144.

(14) Melvin, L. S.; Milne, G. M.; Johnson, M. R.; Subramaniam, B.; Wilken, G. H.; Howlett, A. C. Structure−Activity Relationships for Cannabinoid Receptor-Binding and Analgesic Activity: Studies of Bicyclic Cannabinoid Analogues. *Mol. Pharmacol.* **1993**, *44*, 1008−1015.

(15) Howlett, A. C. Cannabinoid Inhibition of Adenylate Cyclase: Biochemistry of the Response in Neuroblastoma Cell Membranes. *Mol. Pharmacol.* **1985**, *27*, 429−436.

(16) Cheng, Y. C.; Prusoff, W. H. Relationship between the Inhibition Constant (K_i) and the Concentration of Inhibitor which causes 50 Percent Inhibition (IC_{50}) on an Enzymatic Reaction. *Biochem. Pharmacol.* **1973**, *22*, 3099−3108.

(17) Yamada, K.; Rice, K. C.; Flippen-Anderson, J. L.; Eissenstat, M. A.; Ward, S. J.; Johnson, M. R.; Howlett, A. C. (Aminoalkyl)-indole isothiocyanates as potential electrophilic affinity ligands for the brain cannabinoid receptor. *J. Med. Chem.* **1996**, *39*, 1967−1974.

(18) Gasteiger, J.; Marsili, M. Iterative Partial Equalization of Orbital Electronegativity: a Rapid Access to Atomic Charges. *Tetrahedron* **1980**, *36*, 3219−3228.

(19) *Lange's Handbook of Chemistry*; Dean, J. A., Ed.; McGraw-Hill: New York, 1985; pp 5−51.

(20) Wold, S.; Albano, C.; Dunn, W. J., III; Edlund, U.; Esbensen, K.; Geladi, P.; Hellberg, S.; Johansson, E.; Lindberg, W.; Sjostrom, M. Multivariate Data Analysis in Chemistry. In *Chemometrics: Mathematics and Statistics in Chemistry*; Kowalski, B., Ed.; Reidel: Dordrecht, The Netherlands, 1984.

(21) Cramer, R. D., III; Bunce, J. D.; Patterson, D. E. Crossvalidation, Bootstrapping, and Partial Least Squares Compared with Multiple Regression in Conventional QSAR Studies. *Quant. Struct.-Act. Relat.* **1988**, *7*, 18−25.

(22) Devane, W. A.; Dysarz, F. A., III; Johnson, M. R.; Melvin, L. S.; Howlett, A. C. Determination and Characterization of a Cannabinoid Receptor in Rat Brain. *Mol. Pharmacol.* **1988**, *34*, 605−613.

(23) Melvin, L. S.; Milne, G. M.; Johnson, M. R.; Wilken, G. H.; Howlett, A. C. Structure−Activity Relationships Defining the ACD-Tricyclic Cannabinoids: Cannabinoid Receptor Binding and Analgesic Activity. *Drug Des. Discov.* **1995**, *13*, 155−166. (b) Melvin, L. S.; Milne, G. M.; Johnson, M. R.; Subramaniam, B.; Wilken, G. H.; Howlett, A. C. Structure−Activity Relationships for Cannabinoid Receptor-Binding and Analgesic Activity: Studies of Bicyclic Cannabinoid Analogues. *Mol. Pharmacol.* **1993**, *44*, 1008−1015.

(24) Kim, K. H.; Martin, Y. C. Direct Prediction of Linear Free Energy Substituent Effects from 3D Structures Using Comparative Molecular Field Analysis. 1. Electronic Effects of Substituted Benzoic Acids. *J. Org. Chem.* **1991**, *56*, 2723−2729.

(25) Song, Z.-H.; Bonner, T. I. A Lysine Residue of the Cannabinoid Receptor Is Critical for Receptor Recognition by Several Agonists but not WIN55212-2. *Mol. Pharmacol.* **1996**, *49*, 891−896.

JM980305C